Journal of Power Sources 196 (2011) 169–178

Contents lists available at ScienceDirect

Journal of Power Sources

journal homepage: www.elsevier.com/locate/jpowsour

Short communication

# Novel $Nd_2WO_6$-type $Sm_{2-x}A_xM_{1-y}B_yO_{6-\delta}$ (A = Ca, Sr; M = Mo, W; B = Ce, Ni) mixed conductors

Qin Li, Venkataraman Thangadurai*

*Department of Chemistry, University of Calgary, 2500 University Drive NW, Calgary, AB, T2N 1N4, Canada*

ARTICLE INFO

*Article history:*
Received 13 May 2010
Received in revised form 13 June 2010
Accepted 15 June 2010
Available online 23 June 2010

*Keywords:*
Mixed conductors
SOFC anodes
$Sm_{2-x}A_xM_{1-y}B_yO_{6-\delta}$ (A = Ca, Sr
M = Mo, W
B = Ce, Ni)
AC impedance
Blocking electrode

ABSTRACT

In the present work, we have explored novel $Nd_2WO_6$-type structure $Sm_{2-x}A_xM_{1-y}B_yO_{6-\delta}$ (A = Ca, Sr; M = Mo, W; B = Ce, Ni) as precursor for the development of solid oxide fuel cells (SOFCs) anodes. The formation of single-phase monoclinic structure was confirmed by powder X-ray diffraction (PXRD) for the A- and B-doped $Sm_2MO_6$ (SMO). Samples after AC measurements under wet $H_2$ up to 850 °C changed from $Nd_2WO_6$-type structure into $Sm_2MoO_5$ due to the reduction of $Mo^{VI}$ that was confirmed by PXRD and is consistent with literature. The electrical conductivity was determined using 2-probe AC impedance and DC method and was compared with 4-probe DC method. The total electrical conductivity obtained from these two different techniques was found to vary within the experimental error over the investigated temperature of 350–650 °C. Ionic and electronic conductivity were studied using electron-blocking electrodes technique. Among the samples studied, $Sm_{1.8}Ca_{0.2}MoO_{6-\delta}$ exhibits total conductivity of 0.12 S $cm^{-1}$ at 550 °C in wet $H_2$ with an activation energy of 0.06 eV. Ca-doped SMO appears to be chemically stable against reaction with YSZ electrolyte at 800 °C for 24 h in wet $H_2$. The ionic transference number ($t_i$) of $Sm_{1.9}Ca_{0.1}MoO_{6-\delta}$ in wet $H_2$ at 550 °C ($pO_2 = 10^{-25.5}$ atm) was found to be about 0.012 after subtraction of electrical lead resistance from the 2-probe AC data and showed predominate electronic conductors.



## 1. Introduction

A fuel cell is an electrochemical device which directly converts chemical energy into electrical and thermal energies during its operation. Single fuel cell consists of three functional layers such as an ionic conducting electrolyte, and electronic conducting cathode and anode [1,2]. However, several single cells are connected in series using an interconnector, to provide required power density for practical applications. Among the various known fuel cells, the solid oxide fuel cell (SOFC) offers many advantages due to its high operational temperature [1]. It can be operated in various types of fuels, including hydrogen, hydrocarbons (alkanes and alcohols) and biofuels [1,2]. To date, commercial SOFC materials are the $Y_2O_3$-doped $ZrO_2$ (YSZ) electrolyte, Sr-doped $LaMnO_3$ (LSM) cathode, Ni + YSZ cermet composite anode and Sr-doped $LaCrO_3$ interconnector [3–8]. The technology based on these components operates efficiently over the temperature range of about 800–1000 °C [5]. These components show different chemical–physical properties but must have good chemical stability during the operation as well as preparation of SOFCs. Another key element of SOFCs is sealing materials that are stable during the multiple thermal cycling and extend operation period [3,4]. Research is being performed to advance the functionality of these individual materials and primary objectives are improving the performance at as low temperature as possible. Such low-temperature operating SOFCs may simplify current manufacture process which will lower the cost and extend the life time [9,10].

Although, several low-temperature SOFC materials were reported for intermediate temperature (IT) (500–750 °C) SOFCs [6,8,10,11], the development of electrodes, especially anodes that are stable in various impure fuels remains a top priority. The presently used Ni-YSZ cermet anodes play dual role in SOFCs. It not only acts as catalysts for fuel oxidation but also serves as a current collector. There are some disadvantages employing Ni-based anodes, including low tolerance to S, and C formation when exposed to hydrocarbon fuels and poor redox stability [12–14]. The deposited C appears to block the porosity and destroy the microstructure and Ni–YSZ linkages, and causes failure of cell performance. Adsorption of S on Ni forms a poor electronic and ionic conducting and non-catalytic nickel sulphides, which degrade the cell performances. Furthermore, the metal-based anodes tend to agglomerate during the operation which

* Corresponding author. Tel.: +1 403 210 8649; fax: +1 403 289 9488.
*E-mail address:* vthangad@ucalgary.ca (V. Thangadurai).

0378-7753/$ – see front matter © 2010 Elsevier B.V. All rights reserved.
doi:10.1016/j.jpowsour.2010.06.055

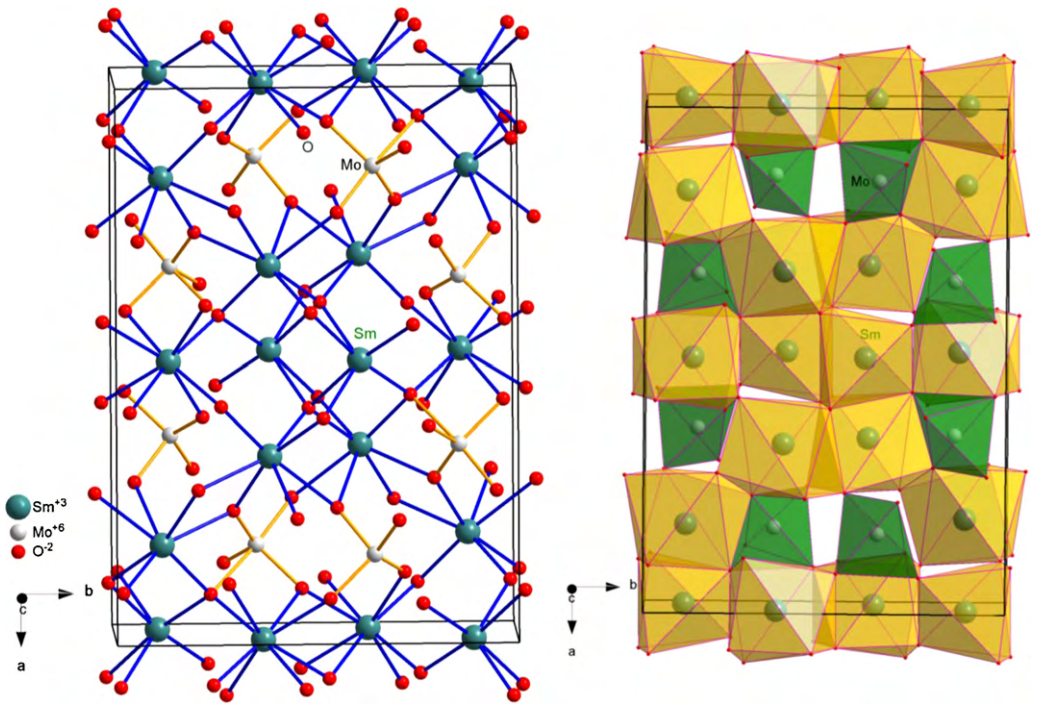


**Fig. 1.** Idealized crystal structure of $Sm_2MoO_6$ showing (left hand side) the connection of $SmO_6$, $SmO_8$ and $MoO_5$ polyhedra and (right hand side) edge sharing of these polyhedra (yellow: $SmO_6$, $SmO_8$; green: $MoO_5$). (For interpretation of the references to color in this figure legend, the reader is referred to the web version of the article.)

decreases the effective triple-phase boundary (TPB). A TPB is an electrochemical active site where the solid electrolyte, a fuel (at the anode) and oxygen (in the case of cathode) molecule, and electrode meet [8]. Hence, the current trend is to replace the conventional cermet with a single-phase metal oxide exhibiting mixed oxide ionic (oxide ion, proton) and electronic conducting materials in SOFCs. This approach is expected to increase the TPB into whole electrode areas which hence increases the electrochemical kinetics. Such anode should have all the desired properties of Ni–YSZ and overcome the limitations. So far, there are no unique materials, including Ni–YSZ, that concurrently meet all the desired physical–chemical properties. Hence, development of SOFCs electrodes remains a challenge for materials chemists.

The goal of the present work is to develop new mixed conductors that possess chemical–physical properties of Ni–YSZ and overcomes the problems. In our earlier work, we reported Mo, and Mo + rare earth-doped ceria as SOFC anode materials [15,16]. These compounds exhibited about three orders of magnitude higher total conductivity in wet $H_2$ compared to that in air at low temperatures due to the reduction of $Mo^{VI}$ and $Ce^{IV}$. In our incessant efforts in searching new anode materials, we have encountered a new family of fluorite-related structure materials with chemical composition of $Sm_2MoO_5$ (SMO) and $Sm_2WO_{6-\delta}$ (SWO) and the former compound can be prepared from the $Nd_2WO_6$-related structure $Sm_2MoO_6$ [17–30] by topochemical reduction in $H_2$ [18]. In Fig. 1, we show the crystal structure of the parent $Sm_2MoO_6$ and it can be described using a linkage of $MoO_5$, $SmO_6$ and $SmO_8$ plolyhedra [31]. In the present work, we have investigated the effect of Ca, Sr-doping for Sm and Ni, Ce-doping for Mo or W sites in SMO and or SWO on electrical conductivity by using 2- and 4-probe DC, and 2-probe AC impedance spectroscopy as a function of temperature in wet $H_2$. These dopants were selected because of comparable ionic radius of the parent metal ions and to generate oxide ion detects in the structure which may affect the electrical conductivity. The electrical conductivity of SMO based materials was found to be about three orders of magnitude higher than that of the corresponding W analogue.

## 2. Experimental

### 2.1. Synthesis and chemical stability

Materials with a nominal chemical formula of $Sm_{2-x}A_xMo_{1-y}M_xO_{6-\delta}$ (A = Ca, Sr; M = Ce, Ni) (SMO) and $Sm_{2-x}A_xW_{1-y}B_yO_{6-\delta}$ (A = Ca; B = Ce) (SWO) were prepared by a conventional solid-state reaction in air using stoichiometric amounts of high purity $CaCO_3$ (Fisher Scientific), $SrCO_3$ (97.5%, Alfa Aesar), $CeO_2$ (>99.9%, Alfa Aesar), NiO (99%, Alfa Aesar), $Sm_2O_3$ (>99.9%, Alfa Aesar), and $MoO_3$ (>99.5%, Alfa Aesar), $WO_3$ (>99.8%, Alfa Aesar). $Sm_2O_3$ were pre-dried in air for at least 48 h at 1000 °C before use. The powders were mixed using a ball mill (Pulverisette, Fritsch, Germany) for 6 h at 150 rpm using zirconia balls and 2-propanol. The mixed powders were then dried and heated in air at 900 °C for 24 h. The resulting mixture was ball-milled using 2-propanol again for about 6 h and then pressed into pellets (~1 cm diameter and ~2 cm length) using isostatic pressure. The pressed green pellets were sintered in air at 1100 °C for 24 h and then 1150 °C for 24 h, with repeated mixing procedures at each step. A few pellets were then ball-milled for powder X-ray diffraction (PXRD) characterization using a Rigaku powder X-ray diffractometer (Cu Kα, 40 kV, 40 mA) at room temperature with a $2\theta$ step scan width of 0.02° and a counting time of 6 s. The lattice constant was determined from the PXRD data by least-squares refinement.

The chemical structure stability of SMO was investigated in wet $H_2$ at 700–900 °C using PXRD. Phase characterization and particle morphology of the pellets after AC measurements in wet $H_2$ up to 850 °C was performed via scanning electron microscopy (SEM) (Philips XL 30). The chemical reactivity of $Sm_{1.9}Ca_{0.1}MoO_{6-\delta}$ with commercial YSZ (Tosoh Corporation, 8TZ) was investigated

at 800 °C in wet $H_2$ for 24 h by combining powders in a 1:1 weight ratio. After the chemical stability reaction, the products were examined by PXRD.

### 2.2. AC impedance spectroscopy

Electrical conductivity measurements were performed on sintered pellets (1150 °C for 24 h) (~0.15 cm in thickness, ~1 cm in diameter) in air, and wet $H_2$ using Pt electrodes. Pt paste (LP A88-11S, Heraeus Inc., Germany) was applied using a paint brush on both sides of the sintered pellets, and cured at 800 °C for 1 h in air to remove the organic binders. Pt wires were attached to the surface of the pellet using a spring-loaded contact, which served as current collectors. The cell was heated to the desired temperature in the range of 300–800 °C using a Barnstead tubular furnace (model 21100) and held at constant temperature for minimum 1 h and maximum 24 h prior to each measurement. The alternating current (AC) impedance spectroscopy (Solartron Electrochemical Impedance Spectroscopy; SI 1260, 100 mV; 0.01 Hz–10 MHz) was used to determine the conductivity. A 2-probe electrochemical cell was employed for the electrical characterization. The conductivity of each sample was measured by subsequent heating and cooling cycles and also tested on different batches of samples to ensure reproducibility.

### 2.3. 2- and 4-Probe DC electrical conductivity

2-Probe DC measurement (Solartron, SI1287 Electrochemical Interface) in wet $H_2$ was made for the $Sm_{1.9}Ca_{0.1}MoO_{6-\delta}$ pellet after AC impedance measurements. The voltage signal varies from 0.05 to 0.6 V. The steady state electronic current as a function of applied voltage was used to determine the electrical conductivity. 4-Probe DC conductivity measurements [32–35] in wet $H_2$ were made using the Princeton applied research, Versa STAT 3 for $Sm_{1.9}Ca_{0.1}MoO_{6-\delta}$. For 4-probe electrical measurements, the samples were polished into a rectangle shape, and then were wrapped with two Pt wires which were held in place by small notches cut on the sample surfaces. Pt paste (LP A88-11S, Heraeus Inc., Germany) was painted on the Pt point contacts and two rectangular cross-sections of the bar sample. The other two Pt wires contacts were made at the cross-sections to act as current contacts. These Pt electrodes and contacts were dried at 150 °C for 1 h in air using a drying chamber and then fired at 800 °C for 1 h to ensure good bonding. A constant current in the range of 0.05–0.5 mA was applied and voltage was measured as a function of time. The result from DC measurements was converted to conductivity using the geometrical factor of the sample.

### 2.4. Determination of transference number

Besides the total electrical conductivity measurement by AC method, ionic conductivity was individually measured for $Sm_{1.9}Ca_{0.1}MoO_{6-\delta}$ by electron-blocking method using 2-probe AC measurements. YSZ was selected as electron-blocking electrode. The test was operated in wet $H_2$ at the temperature range of 550–650 °C. The dense YSZ pellets were obtained by sintering at 1475 °C for 24 h in air after uni-axial pressing. The dense $Sm_{1.9}Ca_{0.1}MoO_{6-\delta}$ pellet for electrical conductivity measurements, with diameters of about 0.7 cm and thickness of about 0.15 cm, were pasted onto YSZ pellets with Pt paste, which was used to overcome the interface resistance. Then, Pt paste was painted to outside of YSZ pellets as current collectors. In the system, the electron flux is blocked by YSZ layer, because YSZ is considered to be almost a pure oxygen ion conductor.

## 3. Results and discussion

### 3.1. Structural characterization of SMO and SWO

Fig. 2 and Fig. S1 and Table S1 (see supporting information) show the PXRD patterns of as-prepared $Sm_{2-x}A_xM_{1-y}B_yO_{6-\delta}$ (A = Ca, Sr; M = Mo, W; B = Ce, Ni) and samples after the AC impedance measurements up to 850 °C. As-prepared samples PXRD

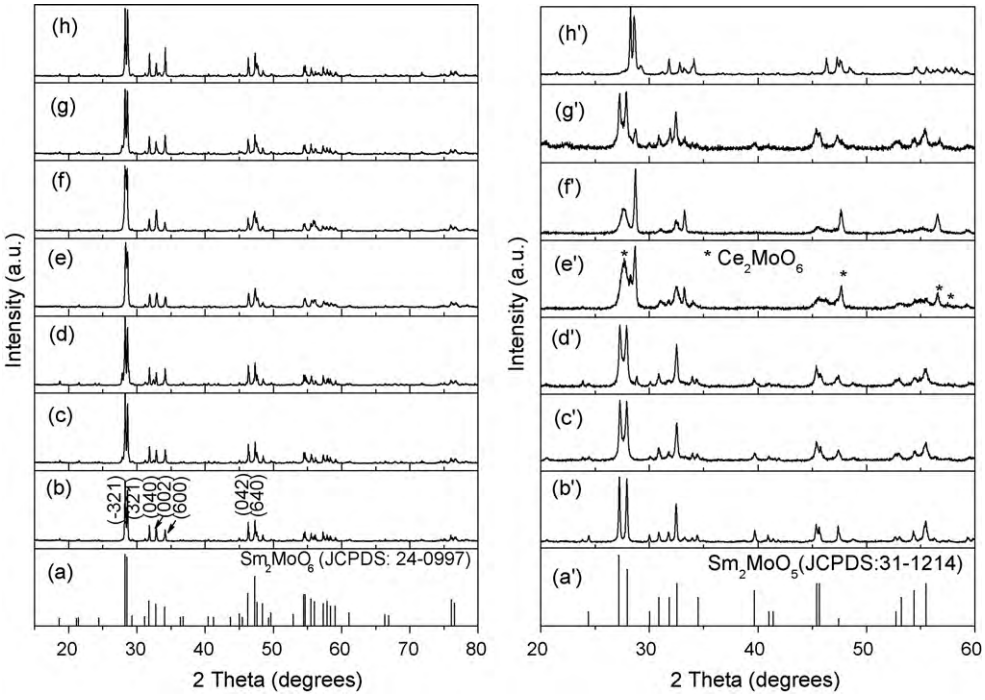


**Fig. 2.** PXRD of (left hand side) (a) $Sm_2MoO_6$ (JCPDS: 24-0997) and as-prepared: (b) $Sm_2MoO_6$, (c) $Sm_{1.9}Ca_{0.1}MoO_{6-\delta}$, (d) $Sm_{1.8}Ca_{0.2}MoO_{6-\delta}$, (e) $Sm_2Mo_{0.9}Ce_{0.1}O_{6-\delta}$, (f) $Sm_2Mo_{0.8}Ce_{0.2}O_{6-\delta}$, (g) $Sm_{1.9}Sr_{0.1}MoO_{6-\delta}$, and (h) $Sm_2Mo_{0.9}Ni_{0.1}O_{6-\delta}$. The PXRD patterns of corresponding sample (a′–h′) after AC impedance measurements in wet $H_2$ are shown in right hand side figure. For comparison $Sm_2MoO_5$ from JCPDS is also shown.

**Table 1**
Indexed PXRD of SMO samples after AC measurement in wet $H_2$.

| $h$ | $k$ | $l$ | $Sm_2MoO_5$[a] | | | $Sm_{1.9}Ca_{0.1}MoO_{5-\delta}$[b] | | | $Sm_{1.9}Sr_{0.1}MoO_{5-\delta}$[c] | | |
|---|---|---|---|---|---|---|---|---|---|---|---|
| | | | $d_{obs}$ (Å) | $d_{cal}$ (Å) | $I_{obs}$ (%) | $d_{obs}$ (Å) | $d_{cal}$ (Å) | $I_{obs}$ (%) | $d_{obs}$ (Å) | $d_{cal}$ (Å) | $I_{obs}$ (%) |
| 2 | 0 | 0 | 3.642 | 3.644 | 12 | 3.642 | 3.644 | 11 | – | – | – |
| 0 | 1 | 3 | 3.274 | 3.275 | 100 | 3.266 | 3.269 | 100 | 3.269 | 3.271 | 98 |
| −2 | 1 | 1 | 3.193 | 3.196 | 98 | 3.195 | 3.195 | 99 | 3.197 | 3.197 | 100 |
| 0 | 0 | 4 | 2.976 | 2.977 | 13 | 2.966 | 2.971 | 11 | 2.976 | 2.973 | 22 |
| 0 | 2 | 0 | 2.895 | 2.897 | 17 | 2.895 | 2.896 | 25 | 2.895 | 2.896 | 32 |
| 0 | 2 | 1 | 2.817 | 2.815 | 17 | 2.810 | 2.813 | 19 | 2.803 | 2.813 | 43 |
| −2 | 0 | 4 | 2.756 | 2.760 | 60 | 2.751 | 2.756 | 64 | 2.758 | 2.758 | 69 |
| −1 | 2 | 0 | 2.692 | 2.692 | 10 | – | – | – | 2.692 | 2.691 | 30 |
| 0 | 2 | 2 | 2.605 | 2.605 | 12 | 2.604 | 2.603 | 15 | – | – | – |
| −2 | 2 | 0 | 2.268 | 2.268 | 20 | 2.270 | 2.267 | 16 | 2.273 | 2.268 | 22 |
| 0 | 1 | 5 | 2.204 | 2.203 | 12 | 2.198 | 2.198 | 11 | 2.200 | 2.200 | 14 |
| −2 | 1 | 5 | 2.180 | 2.181 | 7 | 2.153 | 2.177 | 8 | – | – | – |
| −2 | 2 | 4 | 1.998 | 1.998 | 30 | 1.997 | 1.996 | 35 | 1.998 | 1.998 | 43 |
| 0 | 0 | 6 | 1.987 | 1.985 | 25 | 1.982 | 1.980 | 27 | – | – | – |
| −4 | 0 | 2 | 1.917 | 1.916 | 26 | 1.916 | 1.915 | 22 | 1.921 | 1.917 | 32 |
| 0 | 3 | 3 | 1.737 | 1.737 | 10 | – | – | – | – | – | – |
| −2 | 3 | 1 | 1.726 | 1.725 | 10 | 1.729 | 1.724 | 16 | – | – | – |
| −2 | 1 | 7 | 1.688 | 1.688 | 19 | 1.685 | 1.684 | 20 | 1.685 | 1.685 | 29 |
| 2 | 2 | 4 | 1.656 | 1.657 | 34 | 1.655 | 1.656 | 33 | 1.656 | 1.657 | 43 |

[a] a = 7.662(4) Å; b = 5.794(2) Å; c = 12.518 (4) Å; $\beta$ = 107.97(4).
[b] a = 7.662(4) Å; b = 5.791(3) Å; c = 12.491(5) Å; $\beta$ = 107.96(5).
[c] a = 7.670(5) Å; b = 5.791(2) Å; c = 12.500(3) (4) Å; $\beta$ = 107.94(3).

data was found to be similar to that of the parent compounds $Sm_2MoO_6$ (SMO) (JCPDS: 24-0997) and $Sm_2WO_6$ (SWO) (JCPDS: 23-1401). We did not see major impurity phases in the investigated AO–$Sm_2O_3$–$MoO_3$, $Sm_2O_3$–$MoO_3$–$CeO_2$ and $Sm_2O_3$–$MoO_3$–NiO systems other than that of desired $Nd_2WO_6$-related structure phase. However, we observed small unidentified weak impurity peaks in $Sm_{1.8}Ca_{0.2}WO_6$, $Sm_2W_{0.9}Ce_{0.1}O_6$ and $Sm_2W_{0.8}Ce_{0.2}O_6$ (Fig. S1). Table S2 (see supporting information), we list the various well-known compounds in the investigated system. We could index all the observed diffraction lines of SMO on a monoclinic cell (Table 1 and Table S1) and is consistent with literature (Table S2). We clearly see that lattice constant changes with substitution of alkaline for Sm and Ce or Ni for M in SMO and SWO. In SWO system, we also see very weak impurity peaks due to $Sm_2W_3O_{12}$ (JCPDS Card No. 23-0525) in $Sm_{1.8}Ca_{0.2}WO_{6-\delta}$, $Sm_2W_{0.9}Ce_{0.1}O_{6-\delta}$ and $Sm_2W_{0.8}Ce_{0.2}O_{6-\delta}$. The change in the lattice constant can be understood using Shannon ionic radius [36]. PXRD of the $Sm_{2-x}A_xMoO_{6-\delta}$ (A = Ca, Sr) pellet samples after AC impedance measurements in wet $H_2$ confirmed the formation of $Sm_2MoO_5$ phase (Fig. 2). This can be described using the chemical reaction:

$$Sm_2MoO_6 \xrightarrow{H_2+3\%H_2O} Sm_2MoO_5 + H_2O_{(g)} \quad (1)$$

For $Sm_2Mo_{1-y}Ce_yO_{6-\delta}$ pellet samples after AC measurement in wet $H_2$, multiphase appeared and this can be simply described using the mass un-balanced chemical reaction:

$$Sm_2Mo_{1-y}Ce_yO_{6-\delta} \xrightarrow{H_2+3\%H_2O} Sm_2MoO_6 + Sm_2MoO_5 + Ce_2MoO_6 + H_2O_{(g)} \quad (2)$$

$Sm_2Mo_{1-y}Ni_yO_{6-\delta}$ and SWO retained the original parent $Nd_2WO_6$-type structure after AC measurements in wet $H_2$. We also noticed that for all the samples after AC measurements in wet $H_2$, the colour changed to black from light brownish white, which could be attributed to the reduction $Mo^{VI}$ to lower valence states [17,18]. PXRD showed no evidence of metallic Mo in SMO. The exact oxidation state of Mo in the reduced sample was not investigated. Further characterization involves use of SEM to study the morphology of the SMO pellet samples after AC impedance measurements in wet $H_2$. Fig. 3 shows that typical particle size and density of the investigated materials after AC impedance and samples were found to have porous structure. We also clearly see the excellent particle to particle contact. For comparison, we also included SEM image of corresponding as-prepared compounds in Fig. 4. As-prepared samples showed large sized particles and dense structure, while after AC impedance the size of the particles was found to be decreased, especially for Ca and Sr members. The loss of oxygen due to reduction of $Mo^{VI}$ in the structure and extended sintering during the electrical measurements may cause this microstructure change. However, effect of porosity and microstructure and or particle size on electrical conductivity has not been focused in the present study.

Further chemical stability test of as-prepared powered $Sm_{2-x}A_xMo_{1-y}B_yO_{6-\delta}$ (A = Ca, Sr; B = Ce, Ni) samples was performed in wet $H_2$ and $CH_4$ at 700–900 °C (Figs. S2–S6, see supporting information). For $Sm_{1.9}Ca_{0.1}MoO_{6-\delta}$ and $Sm_{1.9}Sr_{0.1}MoO_{6-\delta}$ after heating in wet $H_2$ and $CH_4$ at 800 °C, $Sm_2MoO_5$ phase was formed, which is consistent with the result from AC measurements. However, both Ce- and Ni-doped $Sm_2Mo_{1-y}B_yO_{6-\delta}$ (B = Ce, Ni) samples showed complex PXRD patterns due to presence of $Sm_2MoO_5$ and $Sm_2MoO_6$-like structures, suggesting partial reduction under the investigated condition. The partial reduction of SMO in $CH_4$ compared to wet $H_2$ may be due to difference in the oxygen partial pressure. Interestingly, unlike Mo-doped $CeO_2$ [15], we did not see the peaks due to metallic Mo in the investigated compounds after chemical stability in $H_2$, which is consistent with literature [17,18].

### 3.2. AC impedance analysis of SMO and SWO

Typical AC impedance plots of SMO and SWO under wet $H_2$ are shown in Fig. 5 and Fig. S7 (see supporting information), respectively. A spike at 1 MHz due to an instrument artifact was found to be consistent with our earlier studies [15,37,38], hence the data points above 1 MHz were omitted for clarity in the figures. In air, the impedance plots can be modeled using an equivalent circuit consisting of three series of parallel resistance–constant phase element contributions $(R_bCPE_b)(R_{gb}CPE_{gb})(R_{el}CPE_{el})$ where $R_b$, $CPE_b$, $R_{gb}$, $CPE_{gb}$, $R_{el}$, and $CPE_{el}$ represent bulk resistance, constant phase element due to bulk, grain-boundary resistance, constant phase element due to grain-boundary, electrode resistance and CPE due to electrode effect, respectively. The line passing through the data points shows the fitted data (Fig. S7). Table S3 (see supporting information) shows the fitting parameter of AC impedance. The magnitude of the pseudo-capacitance ($Q$) values fall in the range

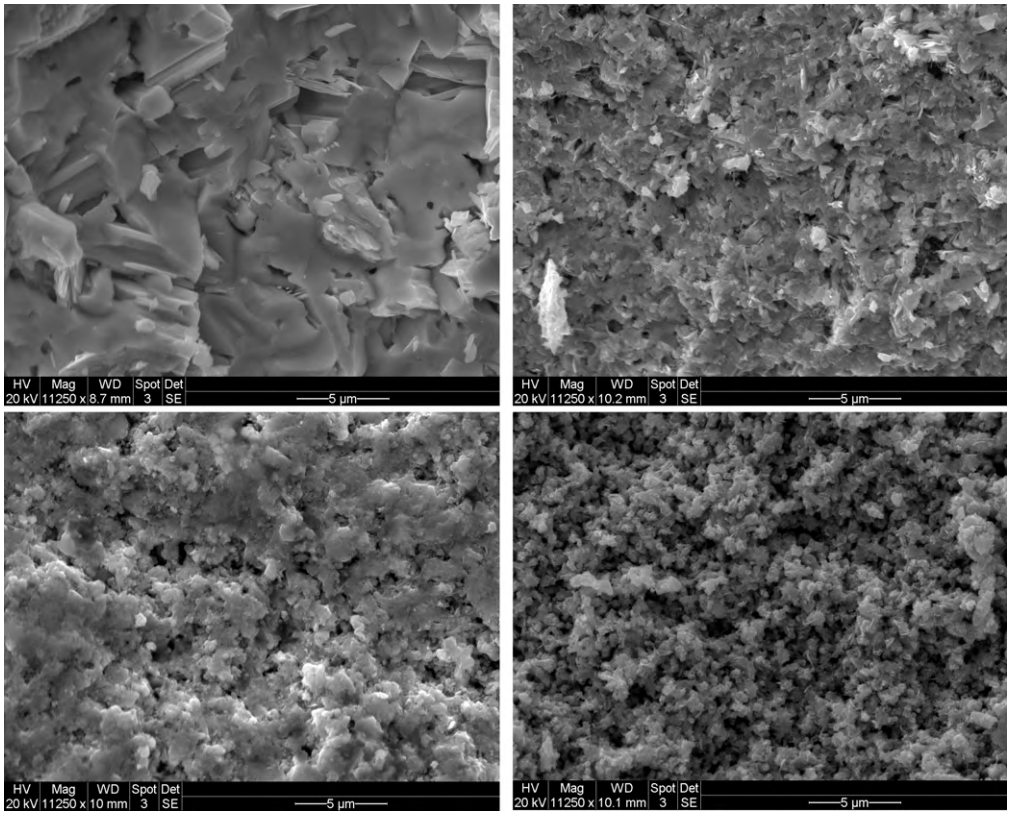


**Fig. 3.** SEM images (5 μm) of (top left) $Sm_2MoO_6$, (top right) $Sm_{1.9}Ca_{0.1}MoO_{6-\delta}$, (bottom left) $Sm_{1.9}Sr_{0.1}MoO_{6-\delta}$ and (bottom right) $Sm_2Mo_{0.9}Ce_{0.1}O_{6-\delta}$, after AC measurement in wet $H_2$ up to 850 °C.

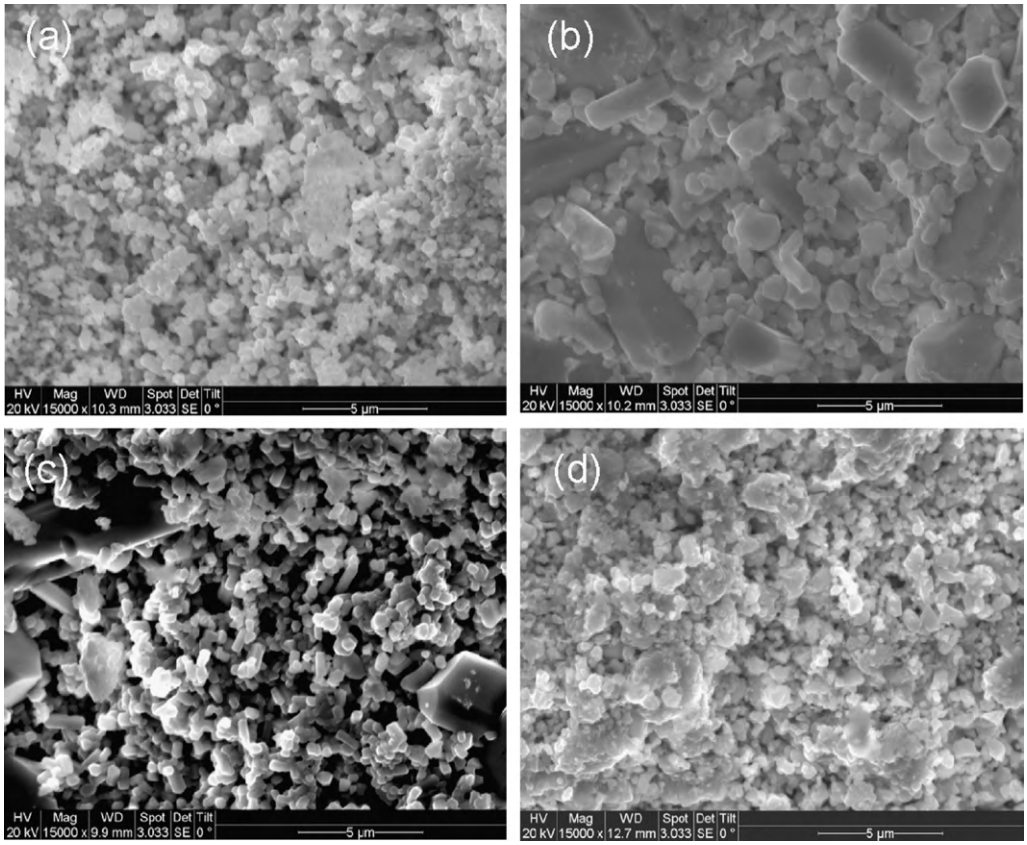


**Fig. 4.** Typical SEM images of as-prepared (a) $Sm_2MoO_{6-\delta}$, (b) $Sm_{1.9}Ca_{0.1}MoO_{6-\delta}$, (c) $Sm_{1.9}Sr_{0.1}MoO_{6-\delta}$ and (d) $Sm_2Mo_{1.9}Ce_{0.1}O_{6-\delta}$.

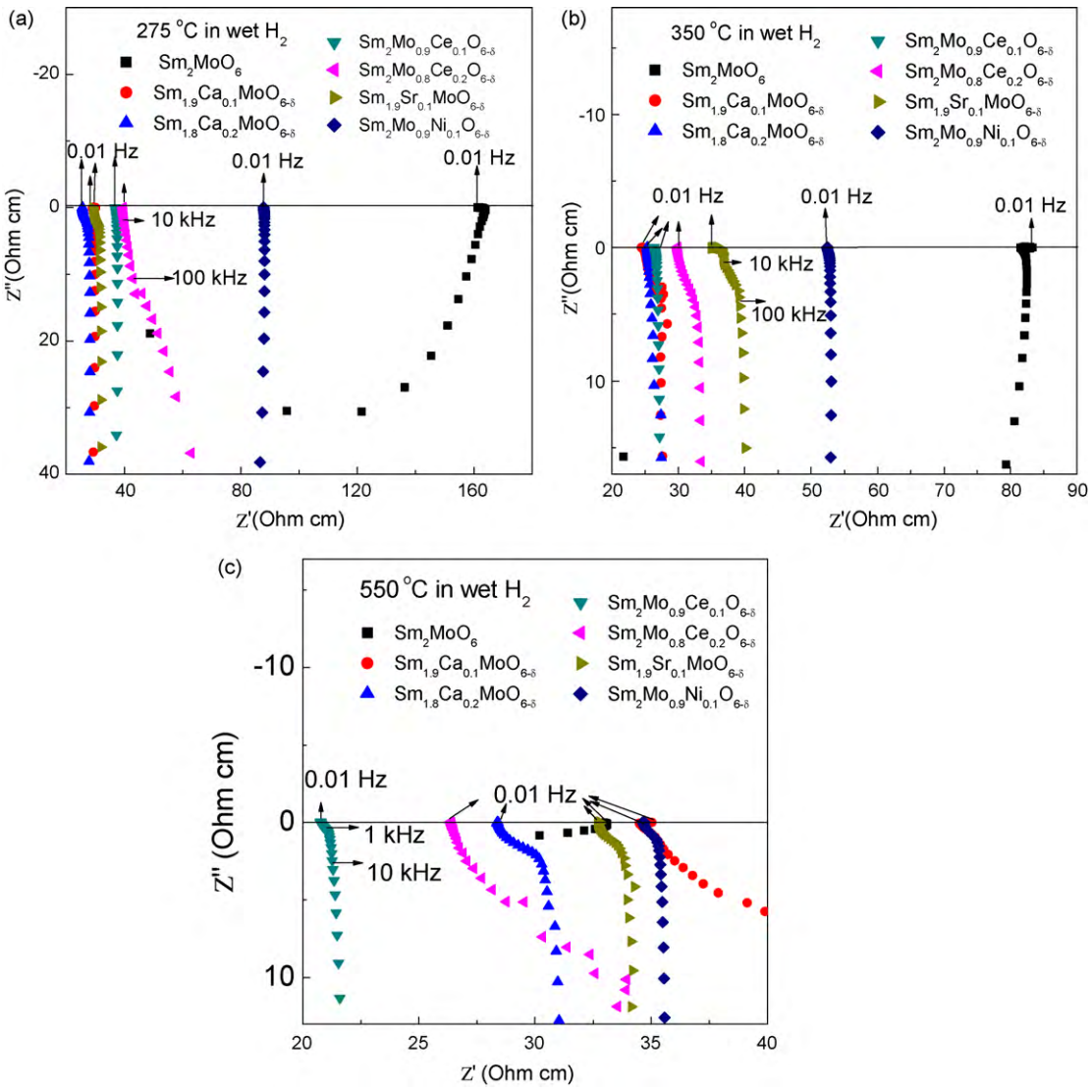


**Fig. 5.** Typical AC resistivity plots of $Sm_{2-x}A_xMo_{1-y}B_yO_{6-\delta}$ (A = Ca, Sr; B = Ce, Ni) at (a) 275 °C, (b) 350 °C and (c) 550 °C in wet $H_2$.

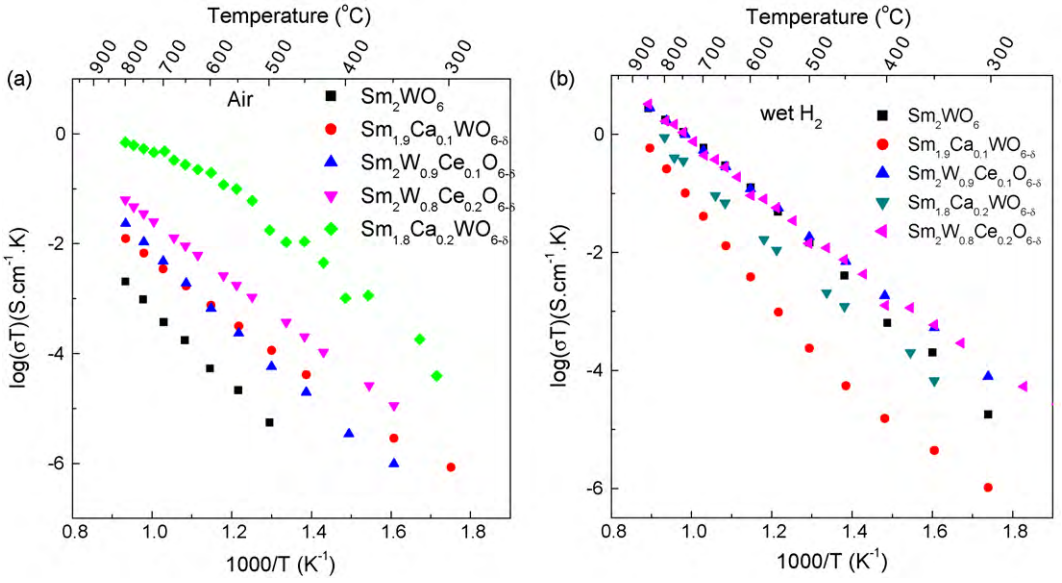


**Fig. 6.** Arrhenius plots for total electrical conductivity of $Sm_{2-x}A_xW_{1-y}B_yO_{6-\delta}$ (A = Ca; B = Ce) in air (a) and in wet $H_2$ (b) determined by 2-probe AC electrical measurements using Pt electrodes.

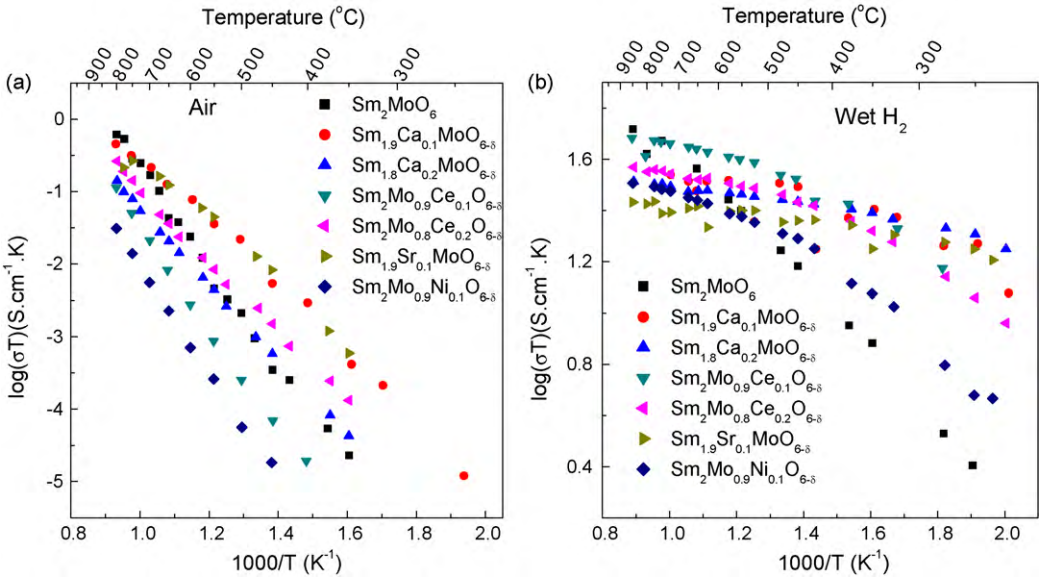


**Fig. 7.** Arrhenius plots for total electrical conductivity of $Sm_{2-x}A_xMo_{1-y}B_yO_{6-\delta}$ (A = Ca, Sr; B = Ce, Ni) in air (a) and in wet $H_2$ (lead contribution has not been subtracted) and (b) determined by 2-probe AC electrical measurements using Pt electrodes. The electrical conductivity obtained from the two or three different batches of samples show slight variation in wet $H_2$, however, it is within the same order of magnitude, and trend in electrical conductivity due to chemical composition is retained.

**Table 2**
Lattice constant and electrical properties of $Sm_{2-x}A_xW_{1-y}B_xO_{6-\delta}$ (A = Ca; B = Ce).

| Compound | Lattice constant of as-prepared material (Å) | | | | $\sigma$ (S cm$^{-1}$) at 550 °C | | $E_a$ (eV) | |
|---|---|---|---|---|---|---|---|---|
| | $a$ | $b$ | $c$ | $\beta$ | Air | Wet $H_2$ | Air | Wet $H_2$ |
| $Sm_2WO_6$[a] | 15.694 (5) | 11.288 (6) | 5.415 (7) | 91.68 (4) | $2.62 \times 10^{-8}$ | $5.92 \times 10^{-5}$ | 1.40 | 1.22 |
| $Sm_{1.9}Ca_{0.1}WO_{6-\delta}$ | 15.114 (7) | 11.439 (8) | 5.247 (12) | 96.17 (8) | $3.86 \times 10^{-7}$ | $1.18 \times 10^{-6}$ | 1.03 | 0.95(250–450 °C)<br>1.66(450–800 °C) |
| $Sm_{1.8}Ca_{0.2}WO_{6-\delta}$ | 15.733 (7) | 11.295 (4) | 5.419 (7) | 91.83 (6) | $1.20 \times 10^{-4}$ | $1.33 \times 10^{-5}$ | 0.60(550–800 °C)<br>1.24(250–550 °C) | 1.17 |
| $Sm_2W_{0.9}Ce_{0.1}O_{6-\delta}$ | 15.720 (10) | 11.195 (7) | 5.4243 (8) | 91.72 (8) | $2.85 \times 10^{-7}$ | $6.81 \times 10^{-5}$ | 1.37 | 1.07 |
| $Sm_2W_{0.8}Ce_{0.2}O_{6-\delta}$ | 15.967 (9) | 11.146 (5) | 5.552 (8) | 89.94 (7) | $2.13 \times 10^{-6}$ | $7.63 \times 10^{-5}$ | 0.96 | 1.01 |

[a] $Sm_2WO_6$ (JCPDS:23-1401): $a$ = 15.731 Å, $b$ = 11.264 Å, $c$ = 5.466 Å, $\beta$ = 91.7.

of about $10^{-11}$–$10^{-4}$ F and these values fall within the range for a characteristic capacitance of the bulk, grain-boundary and electrode contributions to the electrical conducting ceramics. While in wet $H_2$, we see typical resistance behavior for SMO (Fig. 5). We also see positive impedance for imaginary values due to inductance effect in SMO. Such a behavior has been commonly observed at high frequencies when samples are highly conducting. The low-frequency intercept to $Z'$-axis was used to determine the electrical conductivity and it was calculated using the equation: $\sigma = (1/R)(l/a)$ where $R$, $l$ and $a$ represent intercept to $Z'$-axis, thickness and area of the pellet, respectively. The data were plotted using the Arrhenius equation: $\sigma T = A \exp^{(-E_a/KT)}$ (where $E_a$ is the activation energy, $T$ is the temperature and $K$ is the Boltzmann constant) in Figs. 6 and 7.

### 3.3. Electrical properties of SMO and SWO

In air, the electrical conductivity increases with increasing temperature and also substitution of Ca or Sr for Sm and Ce or Ni for

**Table 3**
Lattice constant and electrical properties of $Sm_{2-x}A_xMo_{1-y}B_xO_{6-\delta}$ (A = Ca, Sr; B = Ce, Ni) in air and wet $H_2$.

| Compound | Medium | Lattice constant (Å) | | | | $\sigma$ (S cm$^{-1}$) at 550 °C | $E_a$ (eV) |
|---|---|---|---|---|---|---|---|
| | | $a$ | $b$ | $c$ | $\beta$ | | |
| $Sm_2MoO_6$[a] | Air | 15.760(5) | 11.250(5) | 5.460(2) | 91.01(3) | $5.54 \times 10^{-6}$ | 1.35 |
| $Sm_2MoO_5$ | Wet $H_2$ | 7.662(4) | 5.794(2) | 12.518 (4) | 107.97(4) | $4.13 \times 10^{-2}$ | 0.32 |
| $Sm_{1.9}Ca_{0.1}MoO_{6-\delta}$ | Air | 15.756(7) | 11.234(6) | 5.459(3) | 90.98(4) | $4.33 \times 10^{-5}$ | 0.90 |
| $Sm_{1.9}Ca_{0.1}MoO_5$ | Wet $H_2$ | 7.662(4) | 5.791(3) | 12.491(5) | 107.96(5) | $8.22 \times 10^{-2}$ | 0.08 |
| $Sm_{1.8}Ca_{0.2}MoO_{6-\delta}$ | Air | 15.760(7) | 11.241(5) | 5.458(2) | 91.02(4) | $5.33 \times 10^{-6}$ | 1.03 |
| $Sm_{1.8}Ca_{0.2}MoO_5$ | Wet $H_2$ | 7.664(5) | 5.797(3) | 12.477(7) | 108.01(7) | $1.20 \times 10^{-1}$ | 0.06 |
| $Sm_2Mo_{0.9}Ce_{0.1}O_{6-\delta}$ | Air | 15.760(10) | 11.234(9) | 5.444(6) | 90.81(7) | $1.06 \times 10^{-6}$ | 1.37 |
| | Wet $H_2$ | Multiphase | Multiphase | Multiphase | Multiphase | $1.58 \times 10^{-1}$ | 0.20 |
| $Sm_2Mo_{0.8}Ce_{0.2}O_{6-\delta}$ | Air | 15.765(10) | 11.261(4) | 5.463(4) | 90.98(3) | $1.02 \times 10^{-5}$ | 0.96 |
| | Wet $H_2$ | Multiphase | Multiphase | Multiphase | Multiphase | $1.31 \times 10^{-1}$ | 0.11 |
| $Sm_{1.9}Sr_{0.1}MoO_{6-\delta}$ | Air | 15.763(5) | 11.257(4) | 5.461(2) | 90.98(3) | $5.41 \times 10^{-5}$ | 0.85 |
| $Sm_{1.9}Sr_{0.1}MoO_5$ | Wet $H_2$ | 7.670(5) | 5.791(2) | 12.500(3) | 107.94(3) | $1.14 \times 10^{-1}$ | 0.05 |
| $Sm_2Mo_{0.9}Ni_{0.1}O_{6-\delta}$ | Air | 15.753(6) | 11.248(5) | 5.461(3) | 90.98(3) | $3.16 \times 10^{-7}$ | 1.44 |
| | Wet $H_2$ | 15.778(4) | 11.250(4) | 5.461(2) | 90.96(2) | $7.50 \times 10^{-2}$ | 0.26 |

[a] $Sm_2MoO_6$ (JCPDS:24-0997): $a$ = 15.76 Å, $b$ = 11.26 Å, $c$ = 5.467 Å, $\beta$ = 90.9.

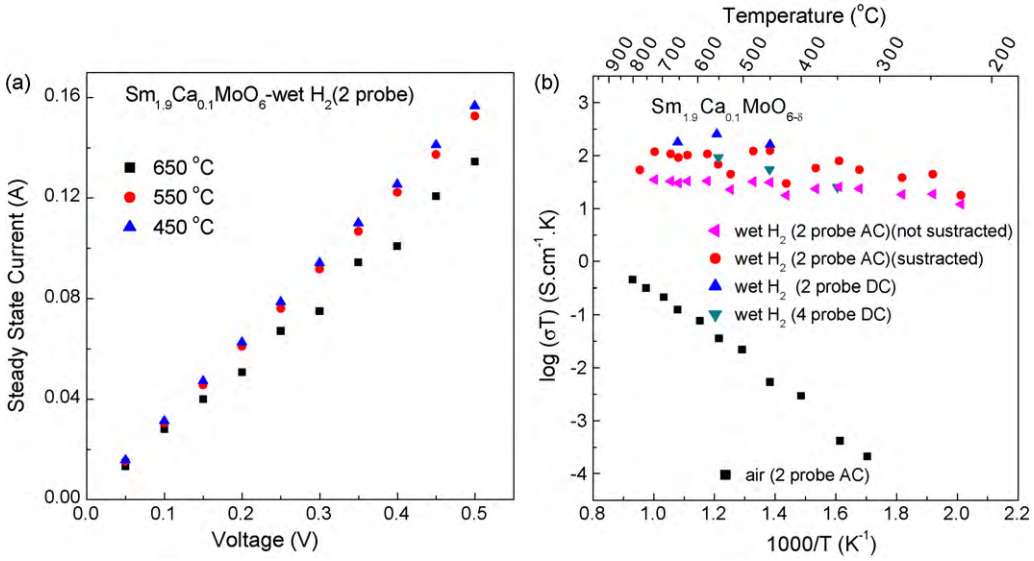


**Fig. 8.** (a) Variation of a steady state electrical current as a function of applied DC potential determined using 2-probe DC measurements for $Sm_{1.9}Ca_{0.1}MoO_{6-\delta}$ in wet $H_2$ at 450–650 °C. It demonstrates a linear dependence, indicative of operation within the ohmic regime. (b) Arrhenius plots for total electrical conductivity of $Sm_{1.9}Ca_{0.1}MoO_{6-\delta}$ in air and wet $H_2$ determined by 2-probe AC electrical measurements using Pt electrodes.

Mo or W except for $Sm_2Mo_{0.9}Ce_{0.1}O_{6-\delta}$ and $Sm_2Mo_{0.9}Ni_{0.1}O_{6-\delta}$ (Tables 2 and 3; Figs. 6 and 7). In air, the increase in electrical conductivity of alkaline earth-doped (Figs. 6a and 7a) compounds compared to that of parent SMO and SWO may be attributed to formation of oxide ion vacancies in the structure. However, the decrease in electrical conductivity of Ce- and Ni-doped SMO may be attributable to second phase in the samples. The activation energy for electrical conduction in air was found to decrease with substitution of Ca and Sr. Also, the Sr member exhibits the lower activation energy compared to that of Ca compound which is consistent with increase in electrical conduction. Among the W and Mo members investigated in the present work, the Mo compound exhibits higher electrical conduction compared to that of the corresponding W analogue. A similar trend has been reported in the double perovskite-like structure [39]. Though the magnitude of activation energy of alkaline-doped SMO and SWO in air was found to be comparable to acceptor-doped fast oxide ion conducting materials such as YSZ (1.1 eV) [40], $La_{0.9}Sr_{0.1}Ga_{0.8}Mg_{0.2}O_{3-\delta}$ (0.73 eV at 700–1000 °C) [41], and $Ce_{0.85}Sm_{0.15}O_{1.925}$ (0.99 eV) [42], the nature of electrical conduction in ambient atmosphere was not investigated in the present work and it was not the primary objective of the present paper.

As anticipated high electrical conductivity was found in wet $H_2$ for SMO compared to that in air, which may be ascribed to reduction of transition metal [18]. The SWO members also showed appreciable increase in electrical conductivity in wet $H_2$. The magnitude of electrical conductivity of SMO was found to be comparable to that reported by Manthiram and Gopalakrishnan [18] who have measured the conductivity using 2-probe DC method in dry $H_2$. The electrical conductivity data obtained during first cycle cooling and second and subsequent cycles follow the same line within the experimental error. In the present work, we also found that electrical conductivity of materials is much higher and AC impedance method may be limited to measure the true conductivity. We have subtracted the resistance of empty cell holders and found that about five time's higher conductivity. Accordingly, we have employed 2-probe and 4-probe DC measurements in wet $H_2$ to determine the electrical conductivity of Ca-doped SMO.

In Fig. S8a, we show variation of electrical current as a function of time for $Sm_{1.9}Ca_{0.1}MoO_{6-\delta}$ at 550 °C for the 2-probe DC measurements in wet $H_2$ with applied potential of 0.1 V and 0.4 V using porous Pt electrodes. For clarity, we have shown both current and time in the log scale. A steady state current seems to be reached within 1 sec and also show almost ohmic nature. Shown in Fig. 8a is variation of a steady state electrical current as a function of applied DC potential for $Sm_{1.9}Ca_{0.1}MoO_{6-\delta}$ in wet $H_2$ at 450–650 °C. It demonstrates a linear dependence, indicative of operation within the ohmic regime and was found to be consistent with AC impedance behavior (Fig. 5). 2-Probe DC electrical conductivity can be simply obtained by product of the slope of $I$ vs. $V$ and cell constant. In Fig. S8b, we show the variation of voltage at constant current as a function of time for $Sm_{1.9}Ca_{0.1}MoO_{6-\delta}$ in wet $H_2$ at 550 °C using the 4-probe DC measurement. The current and voltage in the 4-probe DC measurements can be described using the expression [16,32–34];

$$\sigma_{\mathrm{DC,4\text{-}probe}} = \left(\frac{I}{V}\right)\left(\frac{l}{a}\right)$$

where $l$ and $a$ are the distance between two point contacts and the cross-sectional area of the specimen, respectively. The separation of current and voltage electrodes in 4 probes allows the impedance analyzer to eliminate the impedance contribution of the contact resistances, and this makes more accurate measurements. The total electrical conductivity of $Sm_{1.9}Ca_{0.1}MoO_{6-\delta}$ in wet $H_2$ determined by 2-probe AC electrical measurements using Pt electrodes was found to be comparable (Fig. 8b). The electrical conductivity obtained from these experiments was considered to be total conductivity ($\sigma_t$). The ionic transference number ($t_i$) is defined as the ratio between ionic conductivity and total conductivity.

The electron-blocking electrode technique was used to determine the ionic conductivity. The equilibrium $pO_2$ value was calculated from the assumed chemical equilibrium reaction: $H_2 + 0.5O_2 \rightleftarrows H_2O$. The $t_i$ of $Sm_{1.9}Ca_{0.1}MoO_{6-\delta}$ in wet $H_2$ at 550 °C ($pO_2 = 10^{-28.9}$ atm) and 650 °C ($pO_2 = 10^{-25.5}$ atm) was found to be in the range of $8.7 \times 10^{-3}$–0.03 and 0.012–0.106, respectively, after subtraction of electrical lead contribution. The total electrical conductivity data obtained using AC impedance method was slightly scattered between two sets of samples, and the small difference in resistance will have a great effect on the reported $t_i$ value. If we use 2-probe DC conductivity data instead AC data, the $t_i$ of $Sm_{1.9}Ca_{0.1}MoO_{6-\delta}$ in wet $H_2$ at 650 °C was found to be $5.51 \times 10^{-2}$ after subtraction of lead resistance. Hence, the reported $t_i$ may be

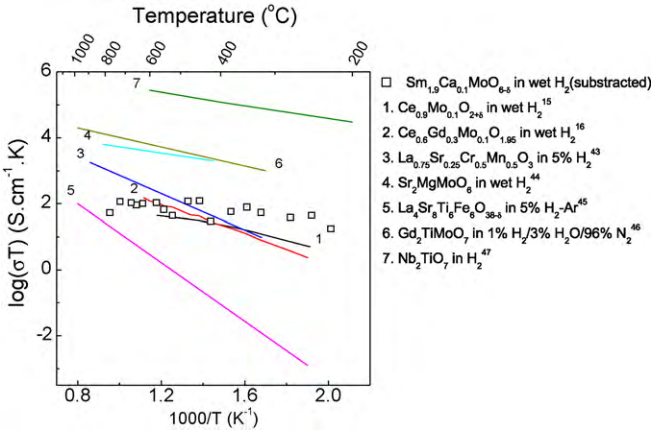


**Fig. 9.** Comparison of electrical conductivity of $Sm_{1.8}Ca_{0.1}MoO_{6-\delta}$ in wet $H_2$ (lead contribution has been subtracted) with other anode materials. (1) $Ce_{0.9}Mo_{0.1}O_{2+\delta}$ in wet $H_2$ [15], (2) $Ce_{0.6}Gd_{0.3}Mo_{0.1}O_{1.95}$ in wet $H_2$ [16], (3) $La_{0.75}Sr_{0.25}Cr_{0.5}Mn_{0.5}O_{3-\delta}$ in 5% $H_2$ [43], (4) $Sr_2MgMoO_{6-\delta}$ in wet $H_2$ [44], (5) $La_4Sr_8Ti_6Fe_6O_{38-\delta}$ in 5% $H_2$–Ar [45], (6) $Gd_2TiMoO_7$ in 1% $H_2$/3%$H_2O$/96%$N_2$ [46], (7) $Nb_2TiO_7$ in $H_2$ [47].

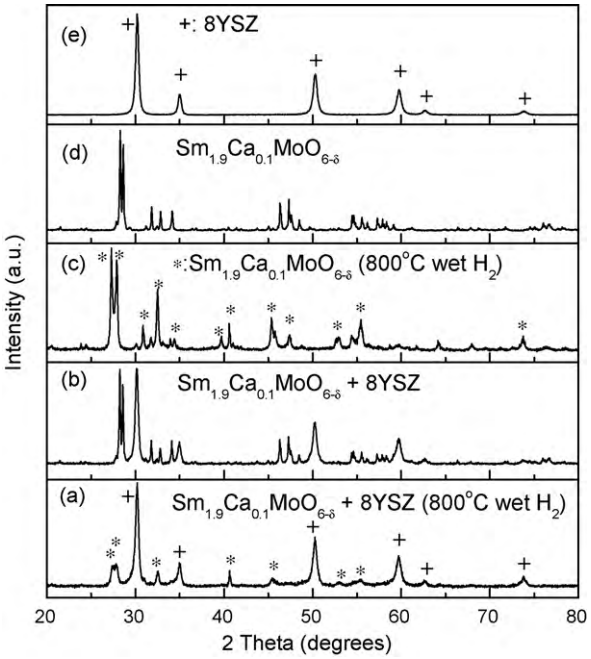


**Fig. 10.** PXRD showing the chemical stability of (a) $Sm_{1.9}Ca_{0.1}MoO_{6-\delta}$ with YSZ after sintering the reaction mixture (1:1 weight ratio) at 800 °C in wet H2 for 24 h. For comparison, (b) the mixture of $Sm_{1.9}Ca_{0.1}MoO_{6-\delta}$ with YSZ, (c) 800 °C wet $H_2$ treated $Sm_{1.9}Ca_{0.1}MoO_{6-\delta}$, (d) as-prepared $Sm_{1.9}Ca_{0.1}MoO_{6-\delta}$ and (e) the starting materials YSZ powders are shown. The biphasic material is clearly shown with + denoting YSZ lines and * denoting 800 °C wet $H_2$ treated $Sm_{1.9}Ca_{0.1}MoO_{6-\delta}$ lines.

considered as an approximate transference number value. Interestingly, this approximate value of Ca-doped SMO was found to be comparable to that of Gd + Mo-doped ceria under the same experimental condition [16]. Based on the preliminary measurements the investigated compounds could be considered as predominate electronic conductors due to very low ionic transference number.

In Fig. 9, we compare the total electrical conductivity of $Sm_{1.8}Ca_{0.2}MoO_{6-\delta}$ with other anode materials reported in the literature [15,16,43–47]. It is interesting to note that the $Sm_{1.9}Ca_{0.2}MoO_{6-\delta}$ exhibits comparable electrical conductivity to that of well-known coke tolerant perovskite-type anode $La_{0.75}Sr_{0.25}Cr_{0.5}Mn_{0.5}O_{3-\delta}$ in 5% $H_2$ [43], and exhibit much higher conductivity compared to $La_4Sr_8Ti_6Fe_6O_{38-\delta}$in 5% $H_2$–Ar [45] over the investigated temperatures. Nonetheless, $Nb_2TiO_7$ [47] still shows much higher conductivity in wet $H_2$ than our investigated sample. We also investigated the chemical reactivity of $Sm_{1.9}Ca_{0.1}MoO_{6-\delta}$ with YSZ electrolyte in wet $H_2$ using PXRD. Fig. 10 shows the PXRD patterns of as-mixed samples and also samples after stability test. The diffraction lines due to electrolyte seem to be retained after the treatment in wet $H_2$, suggesting that reduced $Sm_{1.9}Ca_{0.1}MoO_{6-\delta}$ may be used with YSZ electrolyte for fuel cells and other applications. The weaker peak of reduced $Sm_{1.9}Ca_{0.1}MoO_{6-\delta}$ may be due to low weight ratio compared with YSZ.

## 4. Conclusion

In summary, we have explored new $Nd_2WO_6$-type $Sm_{2-x}A_xM_{1-y}B_xO_{6-\delta}$ (A = Ca, Sr; M = Mo, W; B = Ce, Ni) materials as the new precursors for application in SOFCs. The formation of $Nd_2WO_6$-type structure was confirmed by powder X-ray diffraction (PXRD). Samples after AC measurements under wet $H_2$ up to 850 °C changed from $Nd_2WO_6$-type structure to $Sm_2MoO_5$ due to the reduction of $Mo^{VI}$, which was confirmed by PXRD. The electrical conductivity was determined using 2-probe AC and DC methods and was compared with 4-probe DC method in wet $H_2$. The total electrical conductivity obtained from these different techniques was found to be very close within the experimental error over the investigated temperature of 350–650 °C. Ionic and electronic conductivity were studied using electron-blocking technique. Among the samples studied in this work, $Sm_{1.8}Ca_{02}MoO_{6-\delta}$ compound exhibits the total conductivity of 0.12 S $cm^{-1}$ at 550 °C in wet $H_2$. The electron transference number determined using electron-blocking electrodes decreases with increasing temperature and oxygen partial pressures ($pO_2$).

## Acknowledgements

This research was supported through funding to the NSERC Solid Oxide Fuel Cell Canada Strategic Research Network from the Natural Science and Engineering Research Council (NSERC) and other sponsors listed at www.sofccanada.com. We also would like to thank the NSERC for funding through the Research and Tools (RTI) (cat. 1) and University of Calgary and the Canada Foundation for Innovation (CFI) for the financial support.

## Appendix A. Supplementary data

Supplementary data associated with this article can be found, in the online version, at doi:10.1016/j.jpowsour.2010.06.055.

## References

[1] L. Carrette, K.A. Friedrich, U. Stimming, Fuel Cells 1 (2001) 5–39.
[2] A.B. Stambouli, E. Traversa, Renew. Sust. Energy Rev. 6 (2002) 433–455.
[3] N.Q. Minh, Solid State Ionics 174 (2004) 271–277.
[4] R.M. Ormerod, Chem. Soc. Rev. 32 (2003) 17–28.
[5] A. Lashtabeg, S.J. Skinner, J. Mater. Chem. 16 (2006) 3161–3170.
[6] K.C. Wincewicz, J. Copper, J. Power Sources 140 (2005) 280–296.
[7] H. Koide, Y. Someya, T. Yoshida, T. Maruyama, Solid State Ionics 132 (2000) 253–260.
[8] C.W. Sun, U. Stimming, J. Power Sources 171 (2007) 247–260.
[9] B.C.H. Steele, Solid State Ionics 134 (2000) 3–20.
[10] D.J.L. Brett, A. Atkinson, N.P. Brandon, S.J. Skinner, Chem. Soc. Rev. 37 (2008) 1568–1578.
[11] C.D. Zuo, S.W. Zha, M.L. Liu, M. Hatano, M. Uchiyama, Adv. Mater. 18 (2006) 3318–3320.
[12] A. Atkinson, S. Barnett, R.J. Gorte, J.T.S. Irvine, A.J. Mcevoy, M. Mogensen, S.C. Singhal, J. Vohs, Nat. Mater. 3 (2004) 17–27.
[13] B.C.H. Steele, I. Kelley, H. Middleton, R. Rudkin, Solid State Ionics 28–30 (1988) 1547–1552.
[14] S.W. Tao, J.T.S. Irvine, Chem. Rec. 4 (2004) 83–95.
[15] Q. Li, V. Thangadurai, Fuel Cells 9 (2009) 684–698.

[16] Q. Li, V. Thangadurai, J. Mater. Chem., in press.
[17] E.A. Tkachenko, P.P. Fedorov, Inorg. Mater. 39 (2003) S25–S45.
[18] A. Manthiram, J. Gopalakrishnan, J. Less-Common Met. 68 (1979) 167–174.
[19] M.-H. Chambrier, S. Kodjikian, R.M. Ibberson, F. Goutenoire, J. Solid State Chem. 182 (2009) 209–214.
[20] L.H. Brixner, A.W. Sleight, M.S. Licis, J. Solid State Chem. 5 (1972) 186–190.
[21] P. Urbanowicz, E. Tomaszewicz, T. Groń, H. Duda, A.W. Pacyna, T. Mydlarz, Physica B 404 (2009) 2213–2217.
[22] J.A. Alonso, F. Rivillas, M.J. Martínez-Lope, V. Pomjakushin, J. Solid State Chem. 177 (2004) 2470–2476.
[23] O. Beaury, M. Faucher, G. Teste de Sagey, Acta Crystallogr. B 37 (1981) 1166–1170.
[24] R.A. Rocha, E.N.S. Muccillo, J. Alloys Compd. 400 (2005) 83–87.
[25] J.S. Xue, M.R. Antonio, L. Soderholm, Chem. Mater. 7 (1995) 333–340.
[26] R. Pankajavalli, O.M. Sreedharan, J. Less-Common Met. 171 (1991) 249–254.
[27] H. Kerner-Czeskleba, G. Tourné, Mater. Res. Bull. 13 (1978) 271–278.
[28] F. Lei, B. Yan, H.H. Chen, J. Solid State Chem. 181 (2008) 2845–2851.
[29] F. Lei, B. Yan, J. Am. Ceram. Soc. 92 (2009) 1262–1267.
[30] D.D. Agarwal, K.L. Madhok, H.S. Goswami, React. Kinet. Catal. Lett. 52 (1994) 225–232.
[31] P.V. Klevtsov, L.Y. Kharchenko, R.F. Klevtsovs, Sov. Phys. Crystallogr. 20 (1975) 349–353.
[32] W.S. Wang, A.V. Virkar, Sens. Actuators B 98 (2004) 282–290.
[33] S.P.S. Badwal, J. Mater. Sci. 18 (1983) 3117–3127.
[34] W.S. Wang, A.V. Virkar, J. Power Sources 142 (2005) 1–9.
[35] M.H. Hung, M.V.M. Rao, D.-S. Tsai, Mater. Chem. Phys. 101 (2007) 297–302.
[36] R.D. Shannon, Acta Crystallogr. A 32 (1976) 751–767.
[37] S.S. Bhella, V. Thangadurai, J. Power Sources 186 (2009) 311–319.
[38] R.G. Gerlach, S.S. Bhella, V. Thangadurai, Inorg. Chem. 48 (2009) 257–266.
[39] V. Thangadurai, A.K. Shukla, J. Gopalakrishnan, Solid State Ionics 104 (1997) 277–283.
[40] C.C. Chen, M.M. Nasrallah, H.U. Anderson, Solid State Ionics 70–71 (1994) 101–108.
[41] N. Trofimenko, H. Ullmann, Solid State Ionics 118 (1999) 215–227.
[42] W. Zając, J. Molenda, Solid State Ionics 179 (2008) 154–158.
[43] S.W. Tao, J.T.S. Irvine, Nat. Mater. 2 (2003) 320–323.
[44] Y.H. Huang, R.I. Dass, Z.L. Xing, J.B. Goodenough, Science 312 (2006) 254–257.
[45] J. Canales-Vázquez, J.C. Ruiz-Morales, D. Marrero-López, J. Peña-Martínez, P. Núñez, P. Gómez-Romero, J. Power Sources 171 (2007) 552–557.
[46] P. Holtappels, F.W. Poulsen, M. Mogensen, Solid State Ionics 135 (2000) 675–679.
[47] C.M. Reich, A. Kaiser, J.T.S. Irvine, Fuel Cells 1 (2001) 3–4.